Int. J. Adv. Appl. Math. and Mech. 6(2) (2018) 1 – 13 (ISSN: 2347-2529)

Journal homepage: www.ijaamm.com

International Journal of Advances in Applied Mathematics and Mechanics

A mathematical model of angular two-phase Jeffery Hamel flow in a geothermal pipe

Research Article

Viona Ojiambo[a, *], Mark Kimathi[b], Mathew Kinyanjui[c]

[a] *Department of Pure and Applied Mathematics, Jomo Kenyatta University of Agriculture and Technology, Juja, 62000-00200, Nairobi, Kenya*

[b] *Department of Mathematics, Statistics and Actuarial Science, Machakos University, Machakos, 136-90100, Machakos, Kenya*

[c] *Department of Pure and Applied Mathematics, Jomo Kenyatta University of Agriculture and Technology, Juja, 62000-00200, Nairobi, Kenya*

Received 21 September 2018; accepted (in revised version) 27 November 2018

Abstract: A model of an annular two-phase Jeffrey Hamel flow in a geothermal pipe is designed with silica particles present in the effluent. Thermophoresis is singled out as the source of movement for the particles. The phenomena is also used to determine the growth of silica particles. The power law model has been used to express vicosity in both phases whereby viscosity is a non-linear function of wedge angle in the gaseous phase while a function of wedge angle and temperature in the liquid phase. Equations of mass, momentum, heat transfer and species transfer are the governing equations for this fluid flow. These equations are transformed into nonlinear ordinary differential equations by introducing a similarity transformation. The resulting equations are then solved using the bvp4c MATLAB solver. This method saves on computational time but still provides accurate and convergent results. Skin friction, Nusselt number, Sherwood number, non-dimensional thermophoresis velocity and non-dimensional thermophoresis deposition velocity are determined. The effect of the flow parameters on the flow variables is examined and it is established that changes in velocity and temperature does affect the concentration of silica. An increase in the Reynolds number implies an increase in the fluid velocity which increases the non- dimensional thermophoresis velocity VTW of both the liquid and the gaseous phases. Increase in the VTW implies increased concentration of colloidal silica particles which deposit on the walls of the geothermal pipe.

MSC: 76Dxx • 76Txx

Keywords: Annular Two-phase flow • Non-linear viscosity • Thermophoresis • Mass deposition rate

1. Introduction

Mathematical modelling of geothermal pipe is paramount in providing information on construction and maintenance of geothermal pipes. Geothermal pipe may have different geometries; cylindrically constant, convergent, divergent or elbow shaped. A convergent or divergent point of a geothermal pipe is said to exhibit a Jeffrey-Hamel flow. This flow is characterized with radial direction of flow as established by Polii and Abdurachim [1]. Geothermal pipes are convergent or divergent at certain areas in order to increase or decrease velocity of the geothermal fluid. An example of Jeffrey-Hamel flows in a geothermal pipe from KENGEN geothermal power plant is shown below: Jeffrey[13] and Hamel[14] were the first to discuss the Jeffrey-Hamel flows mathematically. These flows provide an

* Corresponding author.
E-mail address(es): vojiambo@jkuat.ac.ke (Viona Ojiambo), memkimathi@gmail.com (Mark Kimathi), mathewkiny@jkuat.ac.ke (Mathew Kinyanjui).

Fig. 1. Convergent Jeffrey Hamel flow in a geothermal pipe

exact similarity solution of Navier Stokes equations in special case of two-dimensional flow through a channel with inclined plane walls meeting at a vertex having a source or sink. After aforementioned founding work these types of flows have been studied extensively by several authors. Umar and Syed [5] studied flow of a viscous incompressible fluid in a converging-diverging horizontal channel. The system of non-linear partial differential equations was transformed to a system of ordinary differential equations by use of similarity transforms. The method of Variation of Parameters (VPM) was then used to solve the Ordinary Differential Equations. It was established that VPM method is more efficient because it requires less computational time. Gerdroodbary and Ganji [6] studied the influence of thermal radiation on the Jeffrey-Hamel flows. Similarity transformations were used to transform the non-linear partial differential equations to ordinary differential equations. The transformed equations were then solved analytically by applying integral methods. Local skin friction and heat transfer was discussed. It was established that temperatures increases with increase in thermal radiation parameters. K. Umar and Mohyud [7] studied Jeffrey Hamel flow of a non-Newtonian fluid called a Casson fluid. Similarity transforms were applied to reduce the non-linear partial differential equations to Ordinary differential equations. The VPM method and fourth order Runge-Kutta method of were then used to solve the resultant equations. Both methods gave out similar results.

Two phase flows may exist in geothermal pipes. These flows exists when the fluid flow consists of both steam and brine. The fluid flow is said to be of annular flow regime if the steam is centrally placed and brine film is at the wall of the geothermal pipe. An annular flow regime an only occur if the fluid flow is laminar which are characterized by low Reynold's number that are below 2300. Studies on two-phase flows have been done by researchers such as Palsson et al.[3] who established that the stratified wavy flow is the most common type of two phase flow which is dependent on the flow velocity and pressure levels. [21]Alam et al. studied an unsteady two-dimensional laminar forced convective hydrodynamic heat and mass transfer flow of nanofluid along a permeable stretching/shrinking wedge with second order slip velocity using BuongiornoâĂŹs mathematical model. The flow consideration was Jeffrey-Hamel. Using appropriate similarity transformations, the governing non-linear partial differential equations are reduced to a set of non-linear ordinary differential equations which are then solved numerically using the function bvp4c from MATLAB for different values of the parameters. Numerical results for the nondimensional velocity, temperature and nanoparticle volume fraction profiles as well as local skin-friction coefficient, local Nusselt number and local Sherwood number for different material parameters such as wedge angle parameter, unsteadiness parameter, Lewis number, suction parameter, Brownian motion parameter, thermophoresis parameter, slip parameter and Biot number were displayed in graphically as well as tabular form and discussed them from the physical point of view. The obtained numerical results clearly indicate that the flow field is influenced significantly by the second order slip parameter as well as surface convection parameter. Nizami and Sutopo [8] modelled silica scaling deposition in geothermal wells. He was able to come up with a model that predicts silica scaling growth in the two-phase geothermal pipes. Temperature profiles were the most important variable that he considered in his model formulation.

Scaling is a type of sand-like precipitation of dissolved materials that separate from solution, sometimes remaining suspended as small particles or attaching to solid surface such as a pipe wall. Silica scaling could occur in production wells, re-injection wells, turbines and surface pipeline. Areas that converge or diverge are known to have more particle deposition. One of such kind of deposition is silica which polymerizes radially as shown by Nizami and Sutopu [8] who came up with a model that determines the growth of silica deposits by determining the mass deposition rate. Silica deposition results to scaling of geothermal pipe which is one of the major reasons for geothermal pipe losses. Thermophoresis (also thermomigration, thermodiffusion, the Soret effect, or the Ludwig-Soret effect) is a phe-

nomenon observed in mixtures with mobile particles where the different particle types exhibit different responses to the temperature gradient buoyant force caused by temperature gradient. With regards to the geothermal fluid flow, thermophoresis can be defined as the migration of colloidal silica particles present in the geothermal fluid in response to temperature gradient. Thermophoresis is a factor that contributes towards the deposition of silica on the geothermal pipe walls. Studies on thermophoresis have also been of great contribution to research. R. Bosworth and Gimelchin [9] measured the negative force of thermophoretic phenomenon force on a macroscopic spherical particle. Size scaling was done by matching Knudsen numbers to microscale particles such as aerosol droplets at atmospheric pressure. A. Rahman and Uddin [10] performed a numerical study studied of, the influence of magnetic field and thermophoresis on unsteady two-dimensional forced convective heat and mass transfer flow of a viscous, incompressible and electrically conducting fluid along a porous wedge in the presence of the temperature-dependent thermal conductivity and variable Prandtl number. have been studied numerically. He established that the thermophoretic particle deposition velocity is significantly influenced by the magnetic field strength parameter. Moreover, it was found that the rate of heat transfer is significantly influenced by the variation of the thermal conductivity and Prandtl number.[20] Mkwizu et al. investigated the combined effects of thermophoresis, Brownian motion and variable viscosity on entropy generation in a transient generalized Couette flow of nanofluids with Navier slip and convective cooling of water-based nanofluids containing Copper and Alumina as nanoparticles. Both first and second laws of thermodynamics are applied to analyse the problem. The nonlinear governing equations of continuity, momentum, energy and nanoparticles concentration were tackled numerically using a semi discretization finite difference method together with Runge-Kutta Fehlberg integration scheme. Numerical results for velocity, temperature, and nanoparticles concentration profiles were obtained and utilised to compute the entropy generation rate, irreversibility ratio and Bejan number. Pertinent results were displayed graphically and discussed quantitatively. It was established that careful combination of parameter values, the entropy production within the channel flow in a variable viscosity transient generalized Couette flow of nanofluids with Navier slip and convective cooling water based nanofluids can be minimised.

This study models the Jeffrey-Hamel flow of a geothermal fluid with non-linear viscosity and skin friction based on the previous study of Nagler [11] and further extended by [22] Viona et al.; thermophoresis deposition velocity, Skin friction, sherwood number and Nusselt number had not been determined. The body forces comprise of forces due to concentration of silica deposits and temperature gradient. The fluid flow is two-phase with annular flow regime. Nizami and Sutopu[8] model has been used to determine the level of growth of the silica deposits via the determination of thermophoresis deposition velocity. Skin friction, sherwood number and Nusselt number for both phases have also been examined.

2. Mathematical model

Consider a two-phase flow in a geothermal pipe with convergent wedges (non-parallel walls) as shown in the Fig. 1 below.

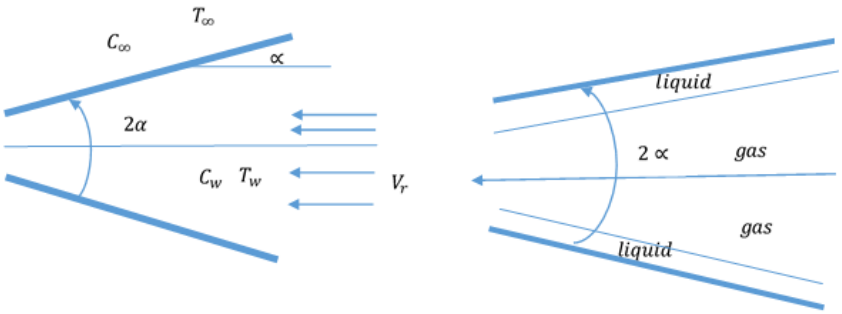

Fig. 2. Flow configuration of a annular two-phase Jeffrey Hamel flow in a geothermal pipe

The fluid is incompressible, two-dimensional and of non-linear viscosity. Further, the fluid flow is unsteady with radial motion that is dependent on r,θ and t. The power law model has been used to govern the non-newtonian behavior of both phases. Viscosity is a non-linear function of T and θ in the liquid phase and a function of θ only in the gaseous state. The fluid is annular with the gaseous phase centrally placed and occupying three fifths of the geothermal fluid in comparison to the liquid which occupies two fifth. Buoyancy forces drive the fluid, viscous dissipation provides the source of energy while thermophoresis enables movement of the silica particles in both phases. Thermophoresis particle deposition is used to determine the growth od silica deposits. The governing equations are equation of mass,

momentum, energy and species transfer.

$C_\infty > C_w$, $T_w > T_\infty$ and I represents the gaseous-liquid inter-phase.Taking an example that $I = \frac{3}{5}\alpha$ which implies that the gaseous phase occupies 60% of the wedge angle while the liquid phase occupies the remaining 40% , Temperature $T = T_w$ decreases by 30% to obtain a value $T = 0.7T_w$ at the inter-phase, concentration $C = C_\infty$ decreases by 30% to obtain a value $C = 0.7C_\infty$ at the inter-phase and velocity decreases by 30% as it approaches the inter-phase

$$\frac{\rho}{r}\frac{\partial}{\partial r}(rV_r) = 0 \tag{1}$$

$$\hat{r} : \rho\left(\frac{\partial V_r}{\partial t} + V_r\frac{\partial V_r}{\partial r}\right) = -\frac{\partial P}{\partial r} + \frac{1}{r}\tau_{rr} + \frac{\partial}{\partial r}(\tau_{rr}) + \frac{1}{r}\frac{\partial}{\partial \theta}(\tau_{\theta r}) - \frac{\tau_{\theta\theta}}{r} + g_r\beta(T - T_\infty) + g_r\beta^\star(C - C_w) \tag{2}$$

$$\hat{\theta} : 0 = -\frac{1}{\rho r}\frac{\partial P}{\partial \theta} + \left(\frac{1}{\rho r^2}\frac{\partial}{\partial r}\left(r^2\tau_{r\theta}\right) + \frac{1}{\rho r}\frac{\partial}{\partial \theta}(\tau_{\theta\theta}) + \frac{\tau_{\theta r} - \tau_{r\theta}}{\rho r}\right) + \frac{g_\theta\beta}{\rho}(T - T_\infty) + \frac{g_\theta\beta^\star}{\rho}(C - C_w) \tag{3}$$

$$\rho C_p\left(\frac{\partial T}{\partial t} + V_r\frac{\partial T}{\partial r}\right) = k_f\left(\frac{1}{r}\frac{\partial}{\partial r}\left(r\frac{\partial T}{\partial r}\right) + \frac{1}{r^2}\frac{\partial^2 T}{\partial \theta^2}\right) + \mu\left(2\left(\frac{\partial V_r}{\partial r}\right)^2 + 2\left(\frac{V_r}{r}\right)^2 + \left(\frac{1}{r}\frac{\partial V_r}{\partial \theta}\right)^2\right) \tag{4}$$

$$\frac{\partial C}{\partial t} + V_r\frac{\partial C}{\partial r} = D\left(\frac{1}{r}\frac{\partial}{\partial r}\left(r\frac{\partial C}{\partial r}\right) + \frac{1}{r^2}\frac{\partial^2 C}{\partial \theta^2}\right) + \frac{1}{r}\frac{\partial}{\partial \theta}(V_{T\theta}C) - \psi C \tag{5}$$

Thermophoretic velocty V_T , was recommended by [15]Talbot et al. and is expressed as:

$$V_T = \frac{-k\nu}{T}\nabla T \tag{6}$$

where $k\nu$ represents the thermophoretic diffusivity and k is the thermophoretic coefficient which ranges in value from 0.2 to 1.2 as indicated by [12] Batchelor and Shen. The power law model has been used to define viscosity as follows:

$$\mu = \mu_0 g^{n-1}, g = g(\theta) \tag{7}$$

where μ is viscosity, μ_0 defines the flow consistency index and n is the flow behavior index. The piecewise definition for viscosity for both the gaseous and the liquid phase are as follows:

$$g = \begin{cases} \theta^s & for\, s \neq 0 \quad (gaseous\ phase) \\ \frac{\theta^s}{1+\gamma(T-T_\infty)} & or\, s\, and\, \gamma \neq 0 \quad (liquid\ phase) \end{cases} \tag{8}$$

where s and γ are constants and θ is the wedge angle.
θ is a subset of angle α. For the total angle 2α of the wedge, $2\alpha = \Omega\pi$. The wedge angle parameter is given by Rahman *et al.* [10]as

$$\Omega = \frac{2m}{m+1} \tag{9}$$

For a convergent Jeffrey-Hamel flow to occur the value of Ω must not exceed 180^0 or π radians. If it exceeds the flow becomes a couette flow.

3. Boundary conditions

The boundary conditions for the above stated model are as follows: For the gaseous phase we have
$\theta\epsilon\left(0, \frac{3}{5}\alpha\right)$

$$V_r = 1 \quad \frac{\partial V_r}{\partial \theta} = 0 \quad T = T_w \quad C = C_w \qquad as \quad \theta = 0$$

$$V_r = 0.3 \qquad T = 0.7T_w \quad C = 0.7 \quad C_\infty \quad as\, \theta = \pm\frac{3}{5}\alpha \tag{10}$$

For the liquid phase we have:
$\theta\epsilon\left(\frac{3}{5}\alpha, \alpha\right)$

$$V_r = 0.3 \quad \frac{\partial V_r}{\partial \theta} = 0 \quad T = 0.7T_w \quad C = 0.7C_\infty \quad as \quad \theta = \pm\frac{3}{5}\alpha$$

$$V_r = 0 \qquad T = T_\infty \quad C = C_\infty \quad as \quad \theta = \pm\alpha \tag{11}$$

4. Similarity transformation

The fluid flow is of potential kind therefore the similarity transform that has been derived from equation of continuity and applied is as follows

$$V_r(\theta,t) = -\frac{Q}{r}\frac{1}{\delta^{m+1}} f(\eta) \tag{12}$$

see [19] Sattar et al. and [11]Naglar et al. m is a parameter that is related to the wedge angle, η is the similarity angle while δ is defined as the time-dependent length scale[more details in [16]Sattar,[17] Alam and Huda and [18] Alam et al.].

$$\delta = \delta(t) \tag{13}$$

Q is the planar volumetric flow rate as defined by [11]Naglar et al.

5. Nondimensionalization

Nondimensionalization is a technique that is used to simplify and parameterize problems where measured units are involved.In this study the following nondimensional variables shall be applied to simplify the problem:

$$\frac{\omega(\eta)}{\delta^{m+1}} = \frac{T - T_\infty}{T_w - T_\infty} \tag{14}$$

$$\frac{\phi(\eta)}{\delta^{m+1}} = \frac{C - C_w}{C_\infty - C_w} \tag{15}$$

where $\frac{\theta}{\alpha} = \eta$ and η is the similarity variable. Employing Eqs. (12), (14) and (15) 15 into Eqs. (1) to (5) we have: For gaseous phase we have:

$$-\left((n-1)\left(s(s-1)\theta^{sn-s-2} + s^2(n-2)\theta^{sn-s-2}\right)\right) f' - s(n-1)\theta^{sn-s-1}\left(2f'' + 4f\right)$$

$$-\theta^{sn-s}\left(4f' + f'''\right) + \frac{2Re}{\delta^{m+1}} f' f - (m+1)\frac{r^{m+1}}{\delta^{m+1}}\lambda f' + \frac{g_r G_{r(T)}}{Q}\left(\omega' - \omega\right) + \frac{g_r G_{r(C)}}{Q}\left(\phi' - \phi\right) = 0 \tag{16}$$

$$\frac{1}{Pr}\omega'' + \frac{r^{m+1}}{\delta^{m+1}}(m+1)\lambda\omega + \frac{Ec\theta^{sn-s}}{r^2\delta^{(m+1)}}\left(4f^2 + \left(f'\right)^2\right) = 0 \tag{17}$$

$$\frac{1}{S_c}\phi'' + (m+1)\frac{r^{m+1}}{\delta^{m+1}}\lambda\phi - \frac{k\theta^{sn-s}}{\left(\omega + N_t\delta^{(m+1)}\right)}\left(\phi'\omega' - \frac{\phi + N_c\delta^{(m+1)}}{\omega + N_t\delta^{(m+1)}}\left(\omega'\right)^2 + \left(\phi + N_c\delta^{(m+1)}\right)\omega'\right)$$

$$-\frac{ks(n-1)\theta^{sn-s-1}}{\delta^{(m+1)}}\left(\frac{\phi + N_c\delta^{(m+1)}}{\omega + N_t\delta^{(m+1)}}\right)\omega' - \frac{\psi}{\delta^{m+1}}\left(\phi + N_c\delta^{(m+1)}\right) = 0 \tag{18}$$

For the liquid phase we have:

$$-(n-1)\left(\frac{\theta^s\delta^{m+1}}{\delta^{m+1} + d\omega}\right)^{n-2}\left(s(s-1)\theta^{s-2} - \frac{d\theta^s\omega' + 2sd\theta^{s-1}\omega'}{\left(\delta^{m+1} + d\omega\right)} - \frac{2\theta^s d^2\left(\omega'\right)^2}{\left(\delta^{m+1} + d\omega\right)^2}\right) f'$$

$$-(n-1)(n-2)\theta^{sn-3s}\left(\frac{\delta^{m+1}}{\delta^{m+1} + d\omega}\right)^{n-2}\left(s\theta^{s-1} - \frac{\theta^s d\omega'}{\left(\delta^{m+1} + d\omega\right)}\right)^2 f'$$

$$-(n-1)\theta^{sn-2s}\left(\frac{\delta^{m+1}}{\delta^{m+1} + d\omega}\right)^{n-1}\left(s\theta^{s-1} - \frac{\theta^s d\omega'}{\left(\delta^{m+1} + d\omega\right)}\right)\left(2f'' + 4f\right)$$

$$-\left(\frac{\theta^s\delta^{m+1}}{\delta^{m+1} + d\omega}\right)^{n-1}\left(4f' + f'''\right) + \frac{2Re}{\delta^{m+1}} f' f - (m+1)\frac{r^{m+1}}{\delta^{m+1}}\lambda f'$$

$$+\frac{g_r G_{r(T)}}{Q}\left(\omega'-\omega\right)+\frac{g_r G_{r(C)}}{Q}\left(\phi'-\phi\right)=0 \tag{19}$$

$$\frac{1}{Pr}\omega''+\frac{r^{m+1}}{\delta^{m+1}}(m+1)\lambda\omega+\frac{Ec\theta^{sn-s}\delta^{(m+1)(n-2)}}{r^2\left(\delta^{m+1}+d\omega\right)^{n-1}}\left(4f^2+\left(f'\right)^2\right)=0 \tag{20}$$

$$\begin{aligned}&\frac{1}{S_c}\phi''+(m+1)\frac{r^{m+1}}{\delta^{m+1}}\lambda\phi\\&-\frac{k}{\left(\omega+N_t\delta^{(m+1)}\right)}\left(\frac{\theta^s\delta^{m+1}}{\delta^{m+1}+d\omega}\right)^{n-1}\left(\phi'\omega'-\frac{\phi+N_c\delta^{(m+1)}}{\omega+N_t\delta^{(m+1)}}\left(\omega'\right)^2+\left(\phi+N_c\delta^{(m+1)}\right)\omega'\right)\\&-\frac{k(n-1)\theta^{sn-2s}}{\delta^{(m+1)}}\left(\frac{\delta^{m+1}}{\delta^{m+1}+d\omega}\right)^{n-1}\left(s\theta^{s-1}-\frac{\theta^s d\omega'}{\left(\delta^{m+1}+d\omega\right)}\right)\left(\frac{\phi+N_c\delta^{(m+1)}}{\omega+N_t\delta^{(m+1)}}\right)\omega'\\&-\frac{\psi}{\delta^{m+1}}\left(\phi+N_c\delta^{(m+1)}\right)=0\end{aligned} \tag{21}$$

Employing Eqs. (12), (14) and (15) the non-dimensionalized boundary conditions are therefore given by:
For the gaseous phase we have:
$\theta\epsilon\left(0,\frac{3}{5}\alpha\right)$

$$f(0)=1\quad f'(0)=0\quad \omega(0)=\delta^{m+1}\quad \phi(0)=0\quad as\quad \eta=0$$

$$f\left(\frac{3}{5}\alpha\right)=0.3\quad \omega\left(\frac{3}{5}\alpha\right)=0.7\delta^{m+1}\quad \phi\left(\frac{3}{5}\alpha\right)=0.7\delta^{m+1}\quad as\quad \eta=\pm\frac{3}{5}\alpha \tag{22}$$

For the liquid phase we have
$\theta\epsilon\left(\frac{3}{5}\alpha,\alpha\right)$

$$f\left(\frac{3}{5}\alpha\right)=0.3\quad f'\left(\frac{3}{5}\alpha\right)=0\quad \omega\left(\frac{3}{5}\alpha\right)=0.7\delta^{m+1}\quad \phi\left(\frac{3}{5}\alpha\right)=0.7\delta^{m+1}\quad as\quad \eta=\pm\frac{3}{5}\alpha$$

$$f(\alpha)=0\quad \omega(\alpha)=0\quad \phi(\alpha)=\delta^{m+1}\quad as\quad \eta=\pm\alpha \tag{23}$$

The non-dimensional numbers obtained from the above equations are: $Re=\frac{Q\rho}{\mu_0}$ is the Reynolds' number, $G_{r(T)}=\frac{\beta r^3(T_w-T_\infty)}{\mu_0}$ is the Grasshoff number due to temperature, $G_{r(C)}=\frac{\beta^\star r^3(C_\infty-C_w)}{\mu_0}$ is the mass Grasshoff number, $Pr=\frac{\mu_0 C_p}{k_f}$ is the Prandtl number, $Ec=\frac{Q^2}{C_p(T_w-T_\infty)}$ is the Eckert number, $Sc=\frac{\mu_0}{D}$ is the Schmidt number, $Nt=\frac{T_\infty}{(T_w-T_\infty)}$ is the thermophoresis parameter and $Nc=\frac{C_w}{(C_\infty-C_w)}$ is the concentration ratio. The unsteadiness parameter is defined by

$$\lambda=\frac{\delta^m}{\nu r^{m-1}}\frac{d\delta}{dt} \tag{24}$$

where

$$\nu=\frac{\mu}{\rho} \tag{25}$$

δ is the the time-dependent length scale, m is a parameter related to the wedge angle and r is the radius of the pipe. Suppose that

$$\lambda=\frac{c}{r^{m-1}} \tag{26}$$

where c is a constant such that

$$c=\frac{\delta^m}{\nu}\frac{d\delta}{dt} \tag{27}$$

Integrating by separation of variables yields:

$$\delta=\left[c(m+1)\nu t\right]^{\frac{1}{m+1}} \tag{28}$$

Taking c=2 and m=1 we obtain

$$\delta=2\sqrt{\nu t} \tag{29}$$

$\delta(t)$ is called a time-dependent length scale because its dimensions are L.

6. Parameters of engineering interest

Skin friction

$$\frac{1}{2}C_f\sqrt{2-\Omega} = Re^{-\frac{1}{2}}f'(0) \tag{30}$$

Nusselt number

$$Nu\sqrt{2-\Omega} = -Re^{-\frac{1}{2}}\omega'(0) \tag{31}$$

Sherwood number

$$Sh\sqrt{2-\Omega} = -Re^{-\frac{1}{2}}\phi'(0) \tag{32}$$

Non-dimensional thermophoretic velocity

$$V_{TW} = -\sqrt{\frac{1}{2-\Omega}}Re^{\frac{1}{2}}\frac{k_f}{1+N_t}\omega'(0) \tag{33}$$

Non-dimensional thermophoretic particle deposition velocity

$$V_d^{\star} = -\sqrt{\frac{1}{2-\Omega}}\frac{1}{Sc}Re^{\frac{1}{2}}\phi'(0) \tag{34}$$

7. Numerical technique

The Collocation technique has been used to solve the resultant ordinary differential equations because it saves on computational time but still provides convergent results that tend to values that previous researchers obtained. This technique has been employed by initiation of the BVP4c MATLAB solver.

8. Results and discussion

Velocity, temperature and concentration have been presented in profiles for both the gaseous and the liquid phase as follows:

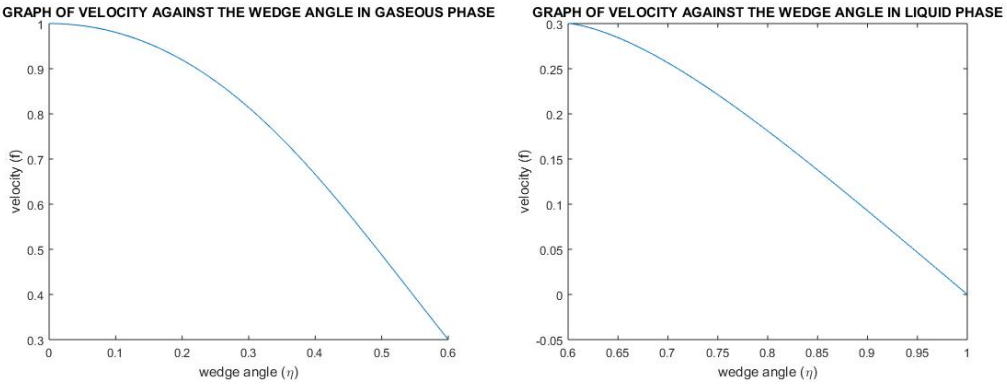

(a) (b)

$Re = 3, \Omega = \frac{1}{3}, Prg = 0.71, Prl = 5.24, Sc = 0.22, Nc = 5, Nt = 5, \varphi = 2, Gr(T) = 0.5, Gr(C) = 0.9$, $k_f = 0.2, Ec = 0.02, \lambda = 1.00$

Fig. 3. Velocity profiles for gaseous and liquid phase

As observed in Fig. 3; at the center of the pipe where the gaseous phase is located there occurs the irrotational flow region where the frictional effects are negligible and the velocity of the gas remains essentially constant in the radial direction of flow. In this region the mass flow rate is a constant implying that the velocity gradient is fully developed. Moving towards the inter-phase the viscous shearing force between the gas and the liquid begin to increase leading to decrease in the velocity of the gaseous phase. At the inter-phase there occurs no-slip condition and the liquid phase acquires the gas velocity. The effects of viscous shearing force are more in the liquid phase compared to the gaseous phase because of high viscosity of the liquid incomparison to the gaseous phase. This is because viscosity is a function of θ in the gaseous phase and a function of T and θ in the liquid phase. Secondly, the frictional are also high in the

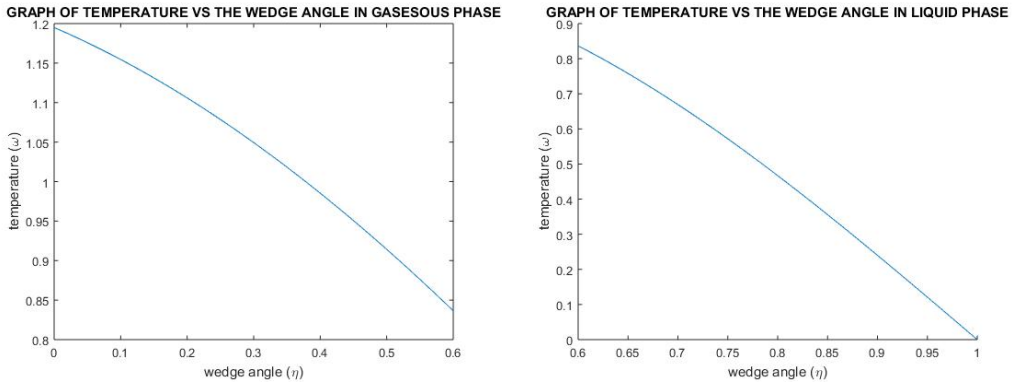

(a)b (b)

$Re = 3, \Omega = \frac{1}{3}, Prg = 0.71, Prl = 5.24, Sc = 0.22, Nc = 5, Nt = 5, \varphi = 2, Gr(T) = 0.5, Gr(C) = 0.9$, $k_f = 0.2, Ec = 0.02, \lambda = 1.00$

Fig. 4. Temperature profiles for gaseous and liquid phase

liquid phase due to its close proximity to the wall of the geothermal pipe. The velocity further decreases as the fluid approaches the wall of the geothermal pipe. At the wall of the of the pipe there occurs no slip condition and the fluid particles in this layer completely come to a stop. The decrease in velocity in both phases is also as a result of relative velocity of the fluid particles and the silica particles. In Fig. 4 temperature at the radial axis T_w is high in comparison to the surface temperature T_∞ which is affected by the environment. At the radial axis the fluid flow is thermally fully developed. This implies that temperature is at its maximum and the effects of the surface temperature due to changes in the environment are negligible. As the wedge angle increases the thermal boundary layer begins to form. In this layer there occurs convection heat transfer as a result of the effects of the surface temperature T_∞ This leads to decrease in temperature.

At the radial axis the gaseous fluid flow is thermally fully developed. As the wedge angle increases the thermal boundary layer begins to form up to the inter-phase where there occurs no slip condition. Further from the inter-phase the thermal boundary layer increases up to the wall of the geothermal pipe. In Fig. 5, concentration of silica

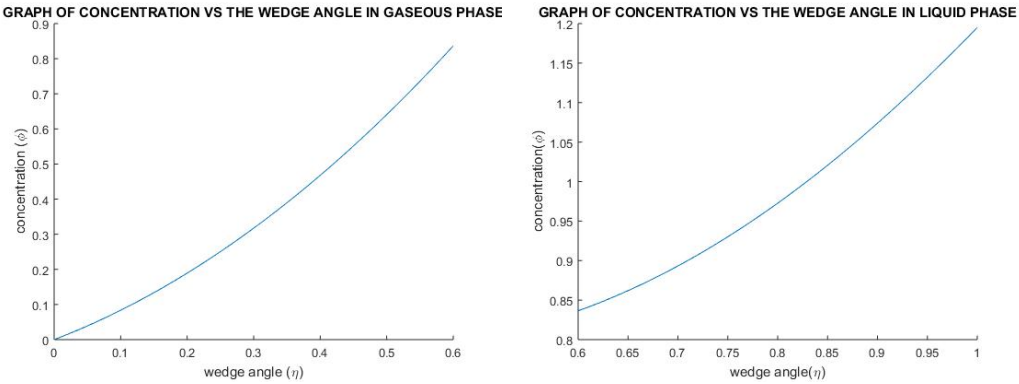

(a) (b)

$Re = 3, \Omega = \frac{1}{3}, Prg = 0.71, Prl = 5.24, Sc = 0.22, Nc = 5, Nt = 5, \varphi = 2, Gr(T) = 0.5, Gr(C) = 0.9$, $k_f = 0.2, Ec = 0.02, \lambda = 1.00$

Fig. 5. Concentration profiles for gaseous and liquid phase

is maximum at the walls because of the deposition of the silica particles. Concentration is a function of temperature while temperature is a function of solubility. From Fig. 4 above, decrease in temperature in the gaseous phase results to decrease in solubility and thermophoresis thereby increasing the amounts of colloidal silica particles. At the inter-phase there occurs no slip of temperature which also influences the concentration of silica. In the liquid phase, the increased concentration of the silica particles is as a result of further decrease in temperature that affects the solubility and thermophoresis of the silica particles which further results to decreased movement of the silica particles; thereby leading to their deposition.

From Fig. 6, the gaseous phase is less viscous in comparison to the liquid phase because viscosity is a non-linear function of θ only in the gaseous phase while it is a function of both θ and T in the liquid phase. The lower the viscous forces the higher the Reynolds number leading to pronounced increase in the gas velocity in comparison to the liquid

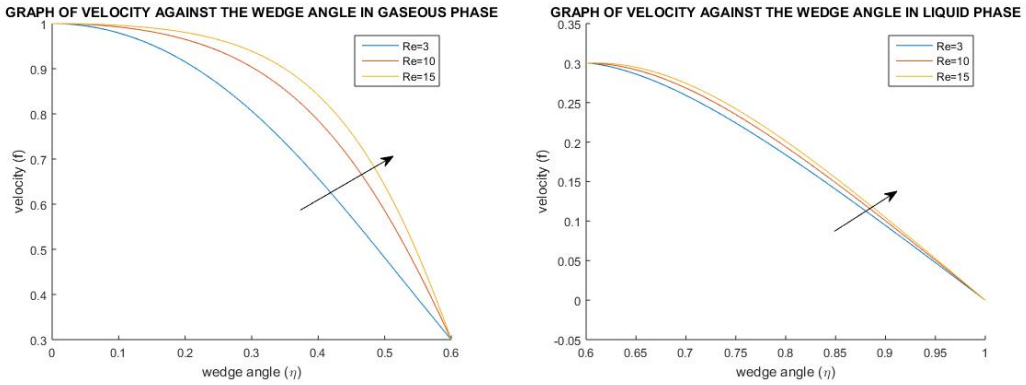

(a) (b)

$$Re = 3, \Omega = \frac{1}{3}, Gr(T) = 0.5, Gr(C) = 0.9$$

Fig. 6. Graph showing the effect of variation of the Reynolds number Re , when λ ,$Gr(T)$ and $Gr(C)$ are held constant

velocity.

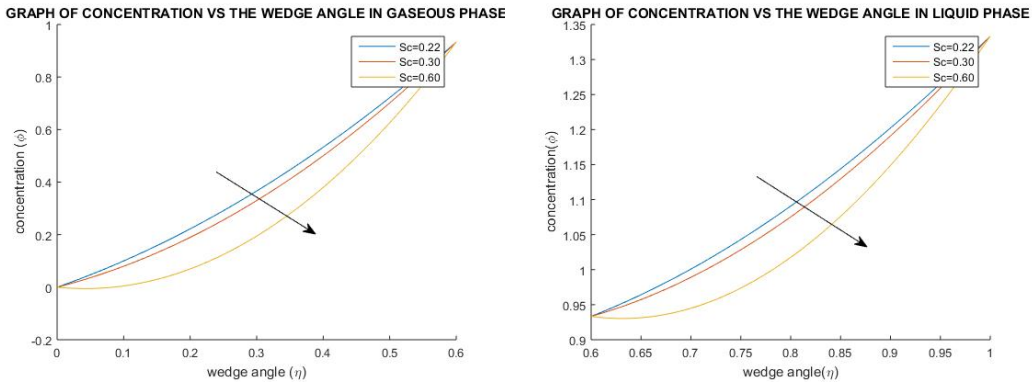

(a) (b)

$$\Omega = \frac{1}{3}, Nc = 5, Nt = 5, \psi = 2, \lambda = 1.00$$

Fig. 7. Graph showing the effects of variation of Schmidt number Sc when λ , Nt , Nc and ψ are held constant

In Fig. 7, increase in the Schmidt number Sc leads to decrease in the mass diffusivity D due to their inverse relationship. Decrease in mass diffusivity implies decreased movement of colloidal silica particles which decreases the concentration of silica particles.

From Fig. 8 increase in the thermophoresis parameter Nt, implies decrease in the temperature difference $(T_w - T_\infty)$. This means that the wall temperature T_∞ is increasing resulting to movement of the silica particles towards the radial axis. This further implies decrease in concentration with increased wedge angle.

In Fig. 9 the methods of preventing silica deposition are given different rank values which can be represented by ψ . The first and the most used rank is flashing the geothermal fluid to pressures below the saturation index, the second rank is to adjust the levels of PH so as to keep silica in solution and therefore present deposition, the third rank is adding condensate to brine to dilute it and prevent super-saturation, the fourth rank is to apply commercially available inhibitors.

Effect of the flow parameters on other flow variables

In this study other flow variables such as skin friction, Nusselt number, Sherwood number, Non-dimensional thermophoretic velocity and the Non-dimensional thermophoretic deposition velocity have been determined at the entry points of the velocity, temperature and concentration profiles. In the Table 1 it is observed that an increase in the Reynolds number Re, when holding Ω constant leads to a decrease in the skin friction C_f , increase in the Nusselt number Nu and a decrease in the Sherwood number Sh in both the liquid and the gaseous phase.

Increase in Reynold's number Re implies decrease in viscous forces. This means that the effects of the boundary layer are decreasing resulting to decrease in the Skin friction drag. The same results can also be justified by Eq. (30)

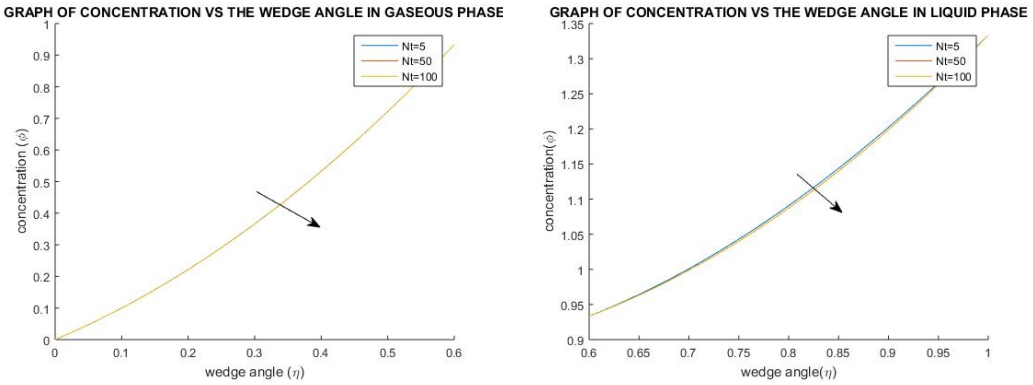

(a) (b)

$$\Omega = \frac{1}{3}, Sc = 0.22, Nc = 5, \psi = 2, \lambda = 1.00$$

Fig. 8. Graph showing the Effects of variation of lambda Nt when Sc , λ , Nc and ψ are held constant

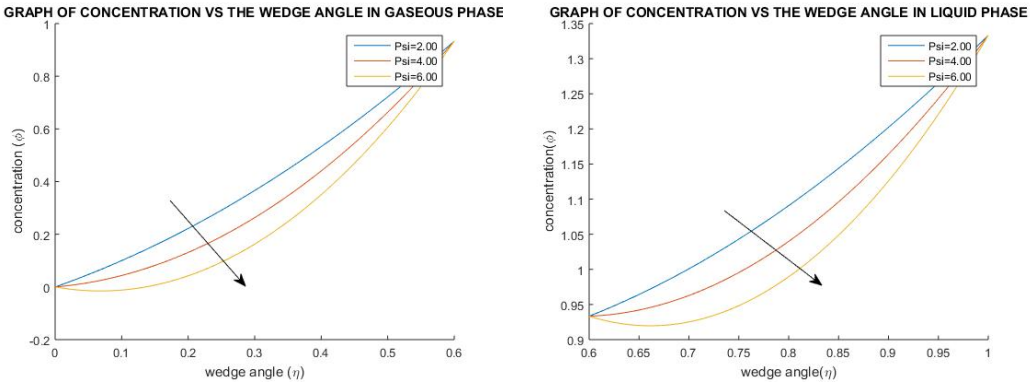

(a) (b)

$$\Omega = \frac{1}{3}, Sc = 0.22, Nc = 5, Nt = 5, \psi = 2, \lambda = 1.00$$

Fig. 9. Graph showing the effects of variation of ψ when Sc , Nt , Nc and λ are held constant

where the Reynold's number Re is inversely proportional to the skin friction C_f. Secondly, decrease in viscous forces also implies that the temperatures of the fluid are increasing resulting to free movement of the fluid molecules. This implies that the rate of heat transferNu is also increasing. Thirdly, since the rate of heat transfer is increasing, it means that the silica particles are becoming soluble thereby their mass transfer rate Sh is decreasing.

In Table 1 it is also observed that an increase in the wedge angle Ω when holding the Reynolds number Re constant leads to an increase in the skin friction C_f in the gaseous phase and a decrease in C_f in the liquid phase, a decrease in the Nusselt number Nu in both phases and an increase in the Sherwood number Sh in both phases.

An increase in Ω implies increase in the volumetric flow rate which results to increased velocity and gas volume fraction. In the liquid phase, increase in velocity implies decrease in the viscous forces that results to decreased skin friction. However, in the increased volume fraction implies that the collision of the gaseous molecules is increasing because they can easily move increasing its viscosity. Also the shifting of the interphase affects the viscosity of the gas because of the no slip condition. This leads to formation of boundary layer that inturn results to increased C_f in the gaseous phase. The Nusselt number Nu decreases because of the convergence that reduces the formation convective current thereby increasing the the concentration of the silica particles as observed through increase in Sherwood number Sh in both phases.

In Table 2 it is observed that an increase in the Reynolds number Re while holding Ω , Nt and k_f constant results to a decrease in the thermophoresis velocity for both the liquid and the gaseous phase. Increase in the Reynolds number Re implies increase in the velocity of the fluid and decrease in the viscous forces. When the fluid is less viscous it implies that the particles within are also dissolved and moving with the fluid. This implies that the thermophoretic velocity V_{TW} is also increasing.

Secondly from Table 2, an increase in the thermophoresis parameter Nt while holding Ω , Re and k_f constant results to a decrease in the thermophoresis velocity in both phases. This is because increase in the thermophoresis parameter Nt implies increases in temperature of the fluid. This decreases the temperature difference thereby decreas-

Table 1. Table showing the effect of Re and Ω on C_f ,Nu and Sh in the gaseous(g) and liquid phase(l)

Re	Ω	C_{fg}	C_{fl}	Nug	Nul	Shg	Shl
3	$\frac{1}{3}$	3.4933	20.2023	-0.1654	-0.6675	0.3334	0.2085
10	$\frac{1}{3}$	0.5697	4.5719	-0.0905	-0.3655	0.1826	0.1142
15	$\frac{1}{3}$	0.2030	0.9013	-0.0739	-0.2984	0.1491	0.0933
3	$\frac{1}{6}$	3.0516	21.7111	-0.1433	-0.5783	0.2632	0.1624
3	$\frac{1}{2}$	3.8750	17.8124	-0.1937	-0.7829	0.4253	0.2690

Table 2. Table showing the effect of Re ,Nt and Ω on V_{TWg} and V_{TWl}

Re	Ω	Nt	k_f	V_{TWg}	V_{TWg}
3	$\frac{1}{3}$	5.0	0.2	-0.0165	-0.0667
10	$\frac{1}{3}$	5.0	0.2	-0.0302	-0.1218
15	$\frac{1}{3}$	5.0	0.2	-0.0370	-0.1492
3	$\frac{1}{3}$	10.0	0.2	-0.0090	-0.0364
3	$\frac{1}{3}$	20.0	0.2	-0.0047	-0.0191
3	$\frac{1}{6}$	5.0	0.2	-0.0143	-0.0578
3	$\frac{1}{2}$	5.0	0.2	-0.0194	-0.0782

ing the thermophoresis velocity. Thirdly, an increase in Ω when holding Re ,Nt and k_f constant results to an increase in the thermophoresis velocity of both phases. This is because of increased velocity of the fluid that implies retention of heat by the two fluids thereby preserving the temperature gradients that results to increased thermophoresis velocity.

Table 3. Table showing the effect of Re ,Nt and Ω on V_{TWg} and V_{TWl}

Re	Ω	Sc	$V^{\star}_{Dg}$	$V^{\star}_{Dl}$
3	$\frac{1}{3}$	0.22	4.5457	2.2436
10	$\frac{1}{3}$	0.22	8.2993	5.1917
15	$\frac{1}{3}$	0.22	10.1646	6.3585
3	$\frac{1}{3}$	0.30	2.2755	1.3816
3	$\frac{1}{3}$	0.60	-0.8309	-0.6248
3	$\frac{1}{6}$	0.22	3.5886	2.2147
3	$\frac{1}{2}$	0.22	5.8002	3.6686

In Table 3 it is observed that an increase in the Reynolds number Re while holding Ω and Sc constant results to a decrease in the non-dimensional thermophoretic particle deposition velocity $V^{\star}_D$ for both phases. This is because of increased movement of gaseous and liquid molecules that reduced the movement of the silica particles leading to decrease in the non-dimensional thermophoretic particle deposition velocity $V^{\star}_D$.
Secondly, an increase in the Schmidt number Sc while holding Ω and Re results to an increase in the deposition velocity in both phases. This is because of decreased diffusion of the liquid and gaseous molecules that results to increased movement of the silica particles leading to increased non-dimensional thermophoretic particle deposition velocity $V^{\star}_D$. Thirdly an increase in the wedge angle Ω when holding Re and Sc constant results to a decrease in the deposition. This is because an increase in the wedge angle allows for increased thermophoresis velocity which increases movement of the liquid and gaseous molecules but decreases the non-dimensional thermophoretic particle deposition velocity $V^{\star}_D$.

The non-dimensional particle deposition velocity $V^{\star}_D$ can be used as the mass deposition rate of silica m_{dep}. This value assists in determining the height(growth) of silica particles as

$$h_s = r - \sqrt{r^2 - \frac{m_{dep}\, t}{\rho_{silica}\pi L}} \tag{35}$$

as defined by Nizami and Sutopu [8]

9. Validation of Results

Comparison of results with Naglar [11] article proved to be in good agreement. It is found that the velocity decreases gradually with the tangential direction progress and Increase in the Reynolds number Re causes the velocity function values to increase. Further the nonlinear viscosity term has influential effects on the flow. These results are observed in both the liquid and the gaseous phase. Similar results were observed with both phases despite adding the buoyancy forces on the momentum equation.
Comparison with Palson *et al.* [3] justifies the existence of two-phase flows in geothermal pipes. Further, the annular flow can only occur in a laminar flow thereby justifying the use of low Reynold's number. From this study.

Nizami and Sutopo [8] affirmed that temperature has the most impact factor that affects mineral solubility of geothermal fluid and cause scaling deposition not only in geothermal wells, but also in surface pipeline, turbines and geothermal wellbore. Other factor such as enthalpy, salinity, and pressure also give impact in changing of solubility of geothermal fluid, but not dominant. In this study thermophoresis has been considered as an influencing factor of scaling deposition. Results from concentration and temperature profiles show an inverse relation. As the temperature increases concentration of colloidal silica particles decreases.

Deposition of silica scaling through the geothermal pipeline is radially[1] and reduce the radius of the well at certain interval time.

10. Conclusion

1. It is paramount to model the governing equations of a two-phase flow separately because their properties are different. In this study a two-phase flow in a geothermal pipe with convergent wedges (non-parallel walls) has been modeled with four governing equations; equation of mass, equation of momentum, equation of energy and equation of concentration.

2. The Reynold's number Re influences the flow velocity, skin friction, Nusselt number and sherwood number. Re significantly influences the viscous forces which impacts on both the thermal and viscous boundary layer.

3. An increase in the Schmidt number Sc leads to decreased mass diffusivity which implies decreased movement of colloidal silica particles which decreases the concentration of silica particles.

4. The non-dimensional particle deposition velocity $V_D^\star$ can be used as the mass deposition rate of silica m_{dep}. This value assists in determining the height(growth) of silica particles.

5. In order to control the rate of heat transfer and mass transfer in the geothermal pipe the walls of the geothermal pipe should not be convergent. There is a lot of deposition and loss of heat that is found in convergent geothermal pipes.

6. The methods of preventing silica deposition are given different rank values which can be represented by ψ . The first and the most used rank is flashing the geothermal fluid to pressures below the saturation index, the second rank is to adjust the levels of PH so as to keep silica in solution and therefore present deposition, the third rank is adding condensate to brine to dilute it and prevent super-saturation, the fourth rank is to apply commercially available inhibitors.

7. Changes in velocity and temperature does affect the concentration of silica. An increase in the Reynolds number implies an increase in the fluid velocity which increases the the non dimensional thermophoresis velocity V_{TW} of both the liquid and the gaseous phase. Increase in the V_{TW} implies increased concentration of colloidal silica particles which deposit on the walls of the geothermal pipe.

Acknowledgements

The author(s) would like to appreciate the Pan African University for Basic Science and Technology for funding of this project. Appreciation also goes to Kenya Electricity Generating Company Limited for giving the authors opportunity to visit the geothermal power plant

References

[1] J. Polii and H. Abdurrachim,Model Development of Silica Scaling Prediction on Brine Flow Pipe, Proceedings, 13th Indonesia International Geothermal Convention and Exhibition, Jakarta, Indonesia, (2013) 12 âĂŞ 14.

[2] A. Hasan and C. Kabir, Modelling two-phase fluid and heat flows in geothermal wells, J. of Petroleum Science and Engineering 71(2003),(2010) 77-86.
[3] H. Palsson, E. Berghorsson and O. Palsson, Estimation and validation of models two phase flow geothermal wells, Proceedings of 10th international symposium of heating and cooling, (2006)
[4] H. Mazumder and A. Siddique, CFD analysis of two-phase flow characteristic in a 90 degree elbow, J. of mechanical engineering. University of Michigan. 3(3) (2011).
[5] K. Umar, A. Naveed, Z. Zaidi , S. Jan and T. Syed, On Jeffrey-Hamel flows, Int. J. of Modern Mathematical Sciences. 7(3)(2013) 236-267.
[6] Gerdroodbary, M. Barzegar, M. Rahimi. and D. Ganji, Investigation of thermal radiation Jeffrey Hamel flow to stretchable convergent/ divergent channels. Science direct, Elsevier case studies in thermal engineering. 6 (2015) 28-39.
[7] K. Umar, A. Naveed, S. Waseen , T. Syed and D. Mohyud, Jeffrey-Hamel flow for a non-Newtonian fluid, J. of Applied and Computational Mechanics. 2(1) (2016) 21-28.
[8] K. Nizami and Sutopo, Mathematical modeling of silica deposition in geothermal wells, 5th International Geothermal Workshop (IIGW2016), IOP Conference series: Earth and Environmental Science (2016)2016
[9] R. Bosworth, A. Ventura, A. Ketsdever and S. Gimelchein, Measurement of negative thermophoretic force, Journal of Fluid Mechanics. 805(2016) 207-221.
[10] A. Rahman, M. Alam and M. Uddin, Influence of magnetic field and thermophoresis on transient forced convective heat and mass transfer flow along a porous wedge with variable thermal conductive and variable thermal conductivity and variable Prandtl number, Int. J. of Advances in Applied Mathematics and Mechanics. 3(4) (2016) 49-64.
[11] J. Nagler J., Jeffrey-Hamel flow on non-Newtonian fluid with nonlinear viscosity and wall friction, J. of Applied Mathematics and Mechanics. 38(6)(2017) 815-830.
[12] G. Batchelor and C. Shen, Thermophoretic deposition of particles in gas flowing over cold surface, J. of colloid interphace science, 107 (1985) 21-37.
[13] G.B. Jeffrey, Two dimensionalsteady motion of a viscous fluid, Philos Mag, 6 (1915) 455-465.
[14] G. Hamel, Spiralformige Bewgugen Zaher Flussigkeiten, Jahresbericht der Deutschen, 25 (1916) 34-60.
[15] L.Talbot, R.Cheng , A. Schefer, D. Wills, Thermophoresis of particles in a heated boundary layer, J. of fluid mechanics. 101 (1980) 737-758.
[16] M. A. Sattar, A local simialrity transformation for the unsteady two-dimensional hydrodynamic boundary layer equations of a flow past a wedge, Int. J. appl.Math. and Mech. 7 (2011) 15-28.
[17] M. S. Alam, M. N. Huda, A new approach for local similarity solutions of an unsteady hydromagnetic free convective heat transfer flow along a permeable flat surface, Int. J. Adv. Appl.Math.Mech. 1(2) (2013) 39-52.
[18] M. S. Alam, M. M. Haque, M. J. Uddin, Unsteady MHD free convective heat transfer flow along a vertical porous flat plate with internal heat generation, Int. J. Adv. Appl.Math.Mech. 2(2) (2014) 52-61.
[19] M. A. Sattar, Derivation of the similarity equation of the 2-D Unsteady Boundary Layer equations and the Corresponding similarity equations, American J. of Fluid Mech. 3(5) (2013) 135-142.
[20] M. H. Mkwizu, A. X. Matofali and N. Ainea, Entropy generation in a variable viscosity transient genralized Coutte flow on nanofluids with Navier Slip and Convective cooling, Int. J. of Adv. in Appied Math. and Mech., 5(4) (2018) 20-29.
[21] M. S. Alam, M. M. Haque and M. J. Uddin, Convective flow of nano fluid along a permeable stretching/shrinking wedge with second order slip using Buongiorno's mathematical model, Int. J. of Adv. in Appied Math. and Mech., 3(3) (2016) 79-91.
[22] V. Ojiambo, M. Kimathi and M. Kinyanjui, A study of two phase Jeffrey Hamel flow in a geothermal pipe, Int. J. of Adv. in Applied Math. and Mech., 5(4) (2018) 21-32.